Study of flow instability in a centrifugal fan based on energy gradient theory[†]

Meina Xiao[1], Qing Xiao[2], Hua-Shu Dou[1,*], Xiaoyang Ma[1], Yongning Chen[3],
Haijiang He[3] and Xinxue Ye[3]

[1]*Faculty of Mechanical Engineering and Automation, Zhejiang Sci-Tech University, Hangzhou, 310018, China*
[2]*Department of Naval Architecture and Marine Engineering, University of Strathclyde, Glasgow, G40LZ, UK*
[3]*Zhejiang Yilida Ventilator Co. Ltd, Taizhou, 318056, China*

Abstract

Flow instability in a centrifugal fan was studied using energy gradient theory. Numerical simulation was performed for the three-dimensional turbulent flow field in a centrifugal fan. The flow is governed by the three-dimensional incompressible Navier-Stokes equations coupled with the RNG k-ε turbulent model. The finite volume method was used to discretize the governing equations and the Semi-implicit method for pressure linked equation (SIMPLE) algorithm is employed to iterate the system of the equations. The interior flow field in the centrifugal fan and the distribution of the energy gradient function K are obtained at different flow rates. According to the energy gradient method, the area with larger value of K is the place where the flow loses stability easier. The results show that instability is easier to generate in the regions of impeller outlet and volute tongue. The air flow near the hub is more stable than that near the shroud. That is due to the influences of variations of the velocity and the inlet angle along the axial direction. With the decrease of the flow rate, instability zone in a blade channel moves to the impeller inlet from the outlet and the unstable regions in different channels develop in opposite direction to the rotation of impeller.

Keywords: Centrifugal fan; Instability; Energy gradient theory; Numerical simulation

---

1. Introduction

Centrifugal fans are widely used in many fields, such as construction, underground engineering and air conditioning. However, the average operating efficiency of the centrifugal fan is far below the national requirements. So the energy-saving potential of the centrifugal fan is very considerable. Due to the influence of rotating impeller and flow viscosity, flow in a centrifugal fan is very complicated. The unstable flow phenomena in the centrifugal fan are the main reason for energy loss and noise increases, including separation, vortex and secondary flow. Therefore, to improve the performance of the centrifugal fan, an in-depth study is needed on the internal flow structure and the mechanism of energy loss.

Much research on the flow field in the centrifugal fan has been done in the aspect of theoretical analysis, experiment and numerical simulation. Denger and Bride [1] observed the strong turbulence near the volute tongue by experiment. Sandra et al. [2] confirmed that the nonuniformity of velocity in the outlet of impeller was determined by flow rate and circum-ferential position. A simulation in the centrifugal fan was done to get the air flow characteristic by Zhu et al. [3]. Wu and Huang [4] analyzed the secondary flow and generation of vortex in the different circumferential cross-section. Chen et al. [5] numerically studied the influence of blade number, blade width and inlet angle on the performance of centrifugal fan. Tamaki [6] confirmed the lumped parameter model was very useful for predicting the influence of piping systems on surge characteristics in centrifugal compressors. Kang et al. [7] found that the motion of volute tongue stagnation and the change of volute tongue throat determined imbalance distribution of velocity in the exit of impeller and the structure with the 62 degree of vortex tongue was the best. On the other hand, Morinushi [8] noted the efficiency is highest when the radius of volute tongue was 0.08 times than the diameter of cylindrical. Computational fluid dynamics and experiments were applied to study the effects of bell mouth geometries on the flow rate of centrifugal blowers by Son et al. [9]. The results showed the bell mouth radius had a greater effect on the flow rate than the gap between the bell mouth and the upper fan case. Son et al. [10] numerically simulated the effect of inlet radius and bell mouth radius on flow rate of centrifugal blower. The inlet radius was revealed to have significant impact on flow rate, but inlet radius and the bell mouth radius did not

have a clear impact on the sound quality of a centrifugal blower. Kim et al. [11] found efficiency was highest when the number of blades was the same in the upper and lower impellers in a forward-curved blade centrifugal fan. Tamaki [12] investigated the prediction accuracy of computational fluid dynamics using a centrifugal compressor whose geometry was intentionally changed to have a distorted flow field over the whole operating range from choke to surge. Ding et al. [13] numerically investigated the flow field in the mixing chamber of the fan and discussed the effect of length of the mixing chamber and the mass flow rate ratio on the fan performance. Jaatinen-Värri et al. [14] experimentally studied seven different vaneless diffuser models for a centrifugal compressor, varying only in diffuser width. The results revealed that the pinch improved the compressor stage and impeller performance but deteriorated the diffuser performance. Kee et al. [15] developed a precise analysis model to investigate the dynamic characteristics of rotating composite blades. It indicates the dynamic characteristics may be significantly influenced by blade curvature, pre-twist, and geometric nonlinearity for shell-type blades.

In summary, researchers always focus on the study of pressure distribution, velocity distribution and the development of vortex, but the mechanism of the vortex and the relationship between the internal flow field and external flow characteristics are not been deeply studied. So the flow structure and the mechanism of energy loss should be further analyzed based on the research of flow characteristic in the centrifugal fan.

We use numerical simulation for the three-dimensional turbulent flow field in the centrifugal fan. The simulation results are consistent with experimental data. The energy gradient theory is applied to analyze the flow stability in the centrifugal fan. The interior flow field and the distribution of the energy gradient function K are obtained at different flow rates and different axial section. According to the contrast of distribution of unstable region and energy gradient function, it is found that the flow in the area with the large value of K loses stability more easily.

2. Energy gradient theory revisited

Dou et al. [16-18] proposed the energy gradient theory to analyze flow instability and turbulent transition. In this theory, the base flow and disturbance determine the critical condition of flow instability, which is agreement with several experimental results. According to the theory, the whole flow field is regarded as an energy field. For a given base flow, fluid particles are periodically perturbed and they gain energy (ΔE) through the disturbance development. At the same time, fluid particles lose energy (ΔH) along the streamline direction because of the fluid viscosity. The flow stability depends on the ratio of the gained energy to the lost energy for a cycle. The larger the cycle number, the higher the ratio. When the ratio exceeds the critical value, fluid instability occurs. As a result, the flow instability criterion for a given flow can be expressed

as follows for a half-period,

$$F = \frac{\Delta E}{\Delta H} = \left(\frac{\partial E}{\partial n} \frac{2\overline{A}}{\pi} \right) \bigg/ \left(\frac{\partial H}{\partial s} \frac{\pi}{\omega_d} u \right)$$
$$= \frac{2}{\pi^2} K \frac{\overline{A}\omega_d}{u} = \frac{2}{\pi^2} K \frac{v'_m}{u} < Const , \tag{1}$$

$$K = \frac{\partial E / \partial n}{\partial H / \partial s} , \tag{2}$$

where F is a function expressing the ratio of the gained energy and the lost energy by the particle in the half-period. K is a dimensionless field function that expresses the ratio of transversal energy gradient, and the rate of the energy loss along the streamline. $E = P + \rho U^2/2$ is the total mechanical energy per unit volumetric fluid, s is along the streamwise direction and n is along the transverse direction. H is the energy loss per unit volumetric fluid along the streamline for finite length. Further, ρ is the fluid density, u is the streamwise velocity of main flow, $\overline{A}$ and ω_d is the amplitude and the frequency of the disturbance respectively, and $v'_m = \overline{A}\omega_d$ is the amplitude of the disturbance of velocity.

From Eqs. (1) and (2), the critical condition of flow instability and turbulence transition is determined by K value. The flow instability first occurs at the region of the maximum of K value, and the instability region becomes larger with the increase of Reynolds number.

The total mechanical energy gradient along the transverse direction can be written as,

$$\frac{\partial E}{\partial n} = \frac{\partial \left(P + 1/2 \rho U^2 \right)}{\partial n} = \frac{\partial P}{\partial n} + \rho U \frac{\partial U}{\partial n} . \tag{3}$$

In the shear flow, the total mechanical energy loss along the streamline direction can be written as,

$$\frac{\partial H}{\partial s} = \frac{\tau}{U} \frac{dU}{dr} - \frac{\tau}{r} . \tag{4}$$

Here, τ is the shear force and it can be written as,

$$\tau = \mu \left(\frac{\partial U}{\partial r} - \frac{U}{r} \right) . \tag{5}$$

Here, μ is the viscosity. For laminar flow, it is the laminar viscosity, and for turbulent flow, it is equal to the sum of laminar viscosity and turbulent viscosity.

The Eq. (4) derived from Eq. (5) can be written as,

$$\frac{\partial H}{\partial s} = \frac{\mu_t}{U} \left(\frac{\partial U}{\partial n} \right)^2 - \frac{2\mu_t}{\rho U^2} \frac{\partial U}{\partial n} \frac{\partial P}{\partial n} + \frac{\mu_t}{\rho^2 U^3} \left(\frac{\partial P}{\partial n} \right)^2 . \tag{6}$$

Thus, the expression of the energy gradient function K can be written as [19],

Table 1. Main geometric parameters of centrifugal fan.

Parameter	Value
Designed flow rate Q_n / (m^3/h)	17126.53
Designed total pressure TP_n / (Pa)	1095
Designed rotational speed N / (r/min)	1500
Impeller inlet diameter D_1 / (mm)	375
Impeller outlet diameter D_2 / (mm)	573
Blade angle at the inlet of impeller β_1 / (°)	26
Blade angle at the outlet of impeller β_2 / (°)	53
Number of blade on each side of impeller Z	12
Blade thickness δ / (mm)	1.2
Rotational direction	(0,1,0)

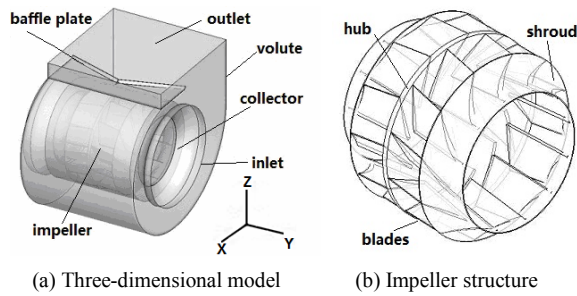(a) Three-dimensional model   (b) Impeller structure

Fig. 1. Centrifugal fan.

$$K = \frac{\partial E / \partial n}{\partial H / \partial s} = \frac{\dfrac{\partial P}{\partial n} + \rho U \dfrac{\partial U}{\partial n}}{\dfrac{\mu_t}{U}\left(\dfrac{\partial U}{\partial n}\right)^2 - \dfrac{2\mu_t}{\rho U^2}\dfrac{\partial U}{\partial n}\dfrac{\partial P}{\partial n} + \dfrac{\mu_t}{\rho^2 U^3}\left(\dfrac{\partial P}{\partial n}\right)^2} \tag{7}$$

The calculation of the energy gradient function K in the flow field is completed by in-house code.

3. Model and grid of centrifugal fan

The centrifugal fan model studied in this paper is based on the backward-curved centrifugal fan belonging to the series of SYH560 in the Zhejiang Yilida Ventilator Co. Ltd. As shown in Fig. 1, it is mainly composed of inlet, collector, impeller, and volute. With respect to the actual model, the inlet and outlet section extend appropriately in the computational domain. The origin of coordinates is located at the center of the hub. In Fig. 1(a), the impeller radial direction along the x direction and the impeller axial direction is along the y direction. The main geometric parameters of the centrifugal fan are as shown in Table 1.

GAMBIT software was used to generate the mesh, and the mesh of the centrifugal fan is shown in Fig. 2. The unstructured tetrahedron mesh was applied to divide the impeller and volute, and structured hexahedral mesh was used to divide the other computational domain. The grid independence was verified on the condition of $Q = 17126.53$ m^3/h and the impeller

Table 2. Check of grid independence.

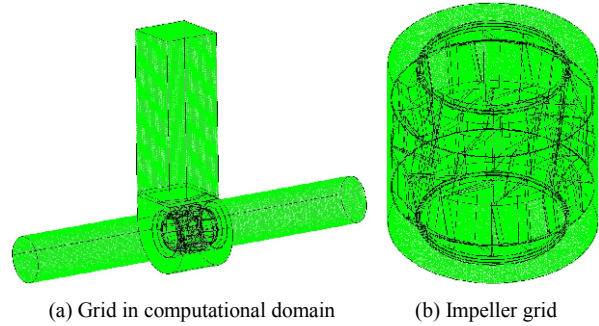| Grid number	Total pressure (TP)
0.87 million	1191.776 Pa
1.48 million	1195.005 Pa
2.82 million	1200.138 Pa

(a) Grid in computational domain   (b) Impeller grid

Fig. 2. Grid of centrifugal fan.

speed $N = 1500$ r/min. The mesh numbers are 0.87 million, 1.48 million and 2.82 million, respectively. It is found that the difference of the Total pressure (TP) is less than 2% as shown in Table 2. The definition of the Total pressure (TP) here is the total pressure difference between the outlet section of the fan and the inlet section of the centrifugal fan. So the density of the grid has little effect on the accuracy of the calculation results when the grid number is larger than 0.87 million. Therefore, the total number of computational domain grid is set to 1.48 million. The grid number is sufficient for the prediction of external characteristics and the internal flow structure in the centrifugal fan. Through the grid quality examination, it is revealed that the grid equal angle skew and equal size skew grid is less than 0.67 and y+ near the wall is about 30. So the grid quality is good.

4. Governing equations and numerical method

The flow is governed by the three-dimensional incompressible Navier–Stokes equations coupled with the RNG k-ε turbulent model. The incompressible Navier-Stokes equations are written as,
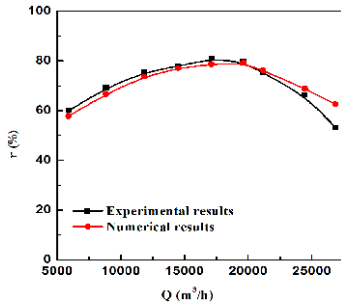
$$\frac{\partial(\rho u_i)}{\partial x_i} = 0, \tag{8}$$

$$\frac{\partial(\rho u_j u_i)}{\partial x_j} = f_i - \frac{\partial P^*}{\partial x_i} + \frac{\partial\left[\mu_e\left(\dfrac{\partial u_i}{\partial x_j} + \dfrac{\partial u_j}{\partial x_i}\right)\right]}{\partial x_j}, \tag{9}$$

where ρ is fluid density, x_j are the components in three directions (x, y, z), u_i are the average velocity components in three directions (u, v, w), P^* is translated pressure including turbulent energy and centrifugal force, f_i are the component of volume force, μ_e is effective viscosity coefficient, and $\mu_e = \mu + \mu_t$, μ
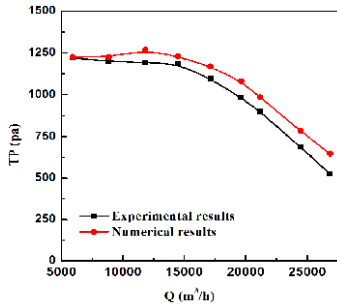
(a)

(b)

Fig. 3. Performance curves of centrifugal fan: (a) curve of *TP* versus flow rate; (b) curve of efficiency versus flow rate.

Fig. 4. Flow channels in the centrifugal fan.
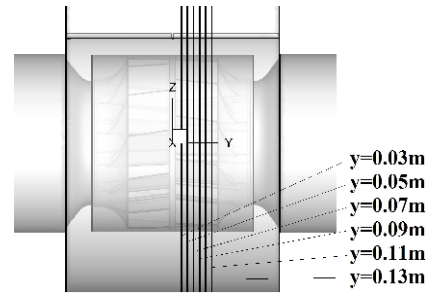
Fig. 5. Axial sections in the centrifugal fan.

is molecular viscosity coefficient, μ_t is turbulent viscosity coefficient and is expressed as,

$$\mu_t = \rho C_\mu \frac{k^2}{\varepsilon}, \quad C_\mu = 0.0845 . \qquad (10)$$

The RNG k-ε turbulent model is represented by the following two equations:

$$\frac{\partial}{\partial t}(\rho k) + \frac{\partial}{\partial x_i}(\rho k u_i)_k$$

$$= \frac{\partial}{\partial x_j}\left(\alpha_k \mu_{eff} \frac{\partial k}{\partial x_j}\right) + G_k + G_b - \rho\varepsilon - Y_M + S_k , \qquad (11)$$

$$\frac{\partial}{\partial t}(\rho\varepsilon) + \frac{\partial}{\partial x_i}(\rho\varepsilon u_i) = \frac{\partial}{\partial x_j}\left(\alpha_\varepsilon \mu_{eff} \frac{\partial\varepsilon}{\partial x_j}\right)$$

$$+ C_{1\varepsilon}\frac{\varepsilon}{k}(G_k + G_{3\varepsilon}G_b) - C_{2\varepsilon}\rho\frac{\varepsilon^2}{k} - R_\varepsilon + S_\varepsilon , \qquad (12)$$

where G_k is the turbulent kinetic energy generated by laminar flow velocity gradient, G_b is the turbulent kinetic energy generated by buoyancy, Y_M is the fluctuation due to diffusion in compressible turbulent flow, $C_{1\varepsilon}$, $C_{2\varepsilon}$ and $C_{3\varepsilon}$ are constants, α_k and α_ε are turbulent Prandtl number in k equation and ε equation, respectively, S_k and S_ε are user-defined.

The finite volume method was used to discretize the governing equations and the SIMPLE algorithm was employed to iterate the system of the equations. The convergence criterion
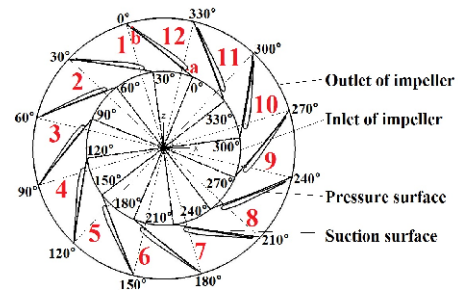
was set that the relative residual was less than 10^{-6} for each variable. The boundary conditions were set as follows. A uniform velocity profile was given at the inlet, and the outflow condition was set at the outlet. No slip boundary condition was applied at the solid wall. The multiple reference frame model was used to define the static region and rotating area.

The flow field was simiulated with commercial software, Fluent. The simulation results of the total pressure and efficiency of the fan were compared with the experimental data and good agreement was achieved as shown in Fig. 3. In Fig. 3(a), the ordinate is the total pressure and the abscissa is the volumetric flow rate, while Fig. 3(b) shows the efficiency versus the volumetric flow rate, In addition to the maximum flow rate condition, the maximum error of total pressure between the experimental data and numerical in other flow conditions is less than 10% and the maximum error of efficiency is less than 4%.

5. Results and discussion

Fig. 4 shows the different blade channels in the axial section of centrifugal fan and different axial sections are shown in Fig. 5. Channel 1 is located at the outlet of the volute and near the volute tongue as shown in red number. The labels of the blade channel are from 2 to 12 along the counterclockwise direction, respectively. The inner circle represents the impeller inlet and the outside circle indicates the outlet. The intersections of two circles and a line extension along the suction surface of the channel 1 are defined as 0° in the circumferential direction. The impeller angular position can be recorded by degrees from 0° to 360° along the counterclockwise direction. For the
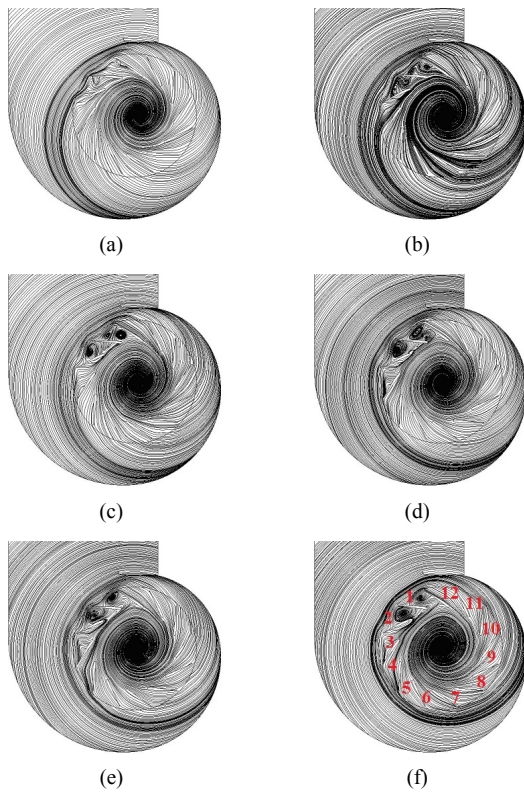
Fig. 6. Streamlines in different axial section for Q/Q_n = 0.69: (a) y = 0.03 m; (b) y = 0.05 m; (c) y = 0.07 m; (d) y = 0.09 m; (e) y = 0.11 m; (f) y = 0.13 m.

Fig. 7. Distribution of K in different axial section for Q/Q_n = 0.69: (a) y = 0.03 m; (b) y = 0.05 m; (c) y = 0.07 m; (d) y = 0.09 m; (e) y = 0.11 m; (f) y = 0.13 m.

points on the suction surface and pressure surface in the blade channel, the front-end and backend of the blade are recorded as a and b. The coordinates of points a and b are set as 0 and 1, then each points on the pressure surface and suction surface can be represented by the number from 0 to 1.

In the centrifugal fan, the air flows from the inlets to the impeller along the axial direction. Then it becomes to radial direction through the impeller. The high-speed air from the impeller collides with volute, and then secondary flow occurs between the impeller and volute. A small portion of air flows back to the impeller through the gap between the shroud and collector. The air flow is influenced by the adverse pressure gradient between the hub and shroud, and the particles with low energy at the hub move to the shroud. So the air speed at the hub is higher than that in the shroud. Then many low energy particles accumulate in the shroud, and the boundary layer near the shroud tends to be thin. At the same time, due to the effect of positive pressure gradient in the radial direction, the fluid is further decelerated and a back flow forms near the blade. Finally, boundary layer separation occurs on the blade surface. After the boundary layer separation, the back flow rises into the mainstream from the blade surface and mixes with the mainstream.

The purpose of this study was to consider the problem of flow instability. Flow instability is generally produced at low flow rate, and not at high flow rate. From Fig. 10, streamlines
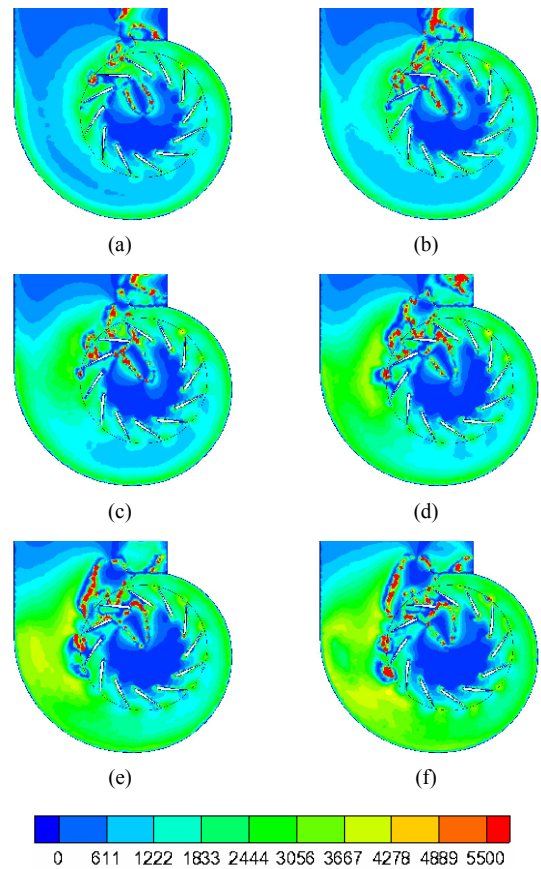
in the axial section of the fan distribute uniformly and no boundary layer separation and flow instability phenomena occur for the large flow condition (Q/Q_n > 1). Fig. 6 shows the streamlines in different axial section for Q/Q_n = 0.69. Here, the designed flow rate Q_n is the flow rate of the fan when the efficiency is highest. It can be seen from Fig. 6(a) that the boundary layer separation first happens near the backend on the suction surface of channels 1 and 2 in the axial section of y = 0.03 m. In Fig. 6(b), two vortices appear in channels 1 and 2, respectively. One is located in the middle of impeller flow channel, and another is located at the outlet of the impeller. In the axial section of y = 0.07 m, the size of the separation vortex increases, and it moves to the inlet of impeller. The separation vortex located at the impeller outlet becomes larger and occupies the whole channel gradually. At the same time, another separation vortex is squeezed and becomes smaller. As can be seen in Figs. 6(c) and (d), the streamlines in channel 3 are not smooth, which indicates that the boundary layer separation would occur. Continuing close to the shroud, two separation vortices in channels 1 and 2 are reduced to one and the streamlines are bent in channels 3 and 4 in Figs. 6(e) and (f).

Through the above analysis, we can see the boundary layer separation first occurs at the trailing edge of suction surface
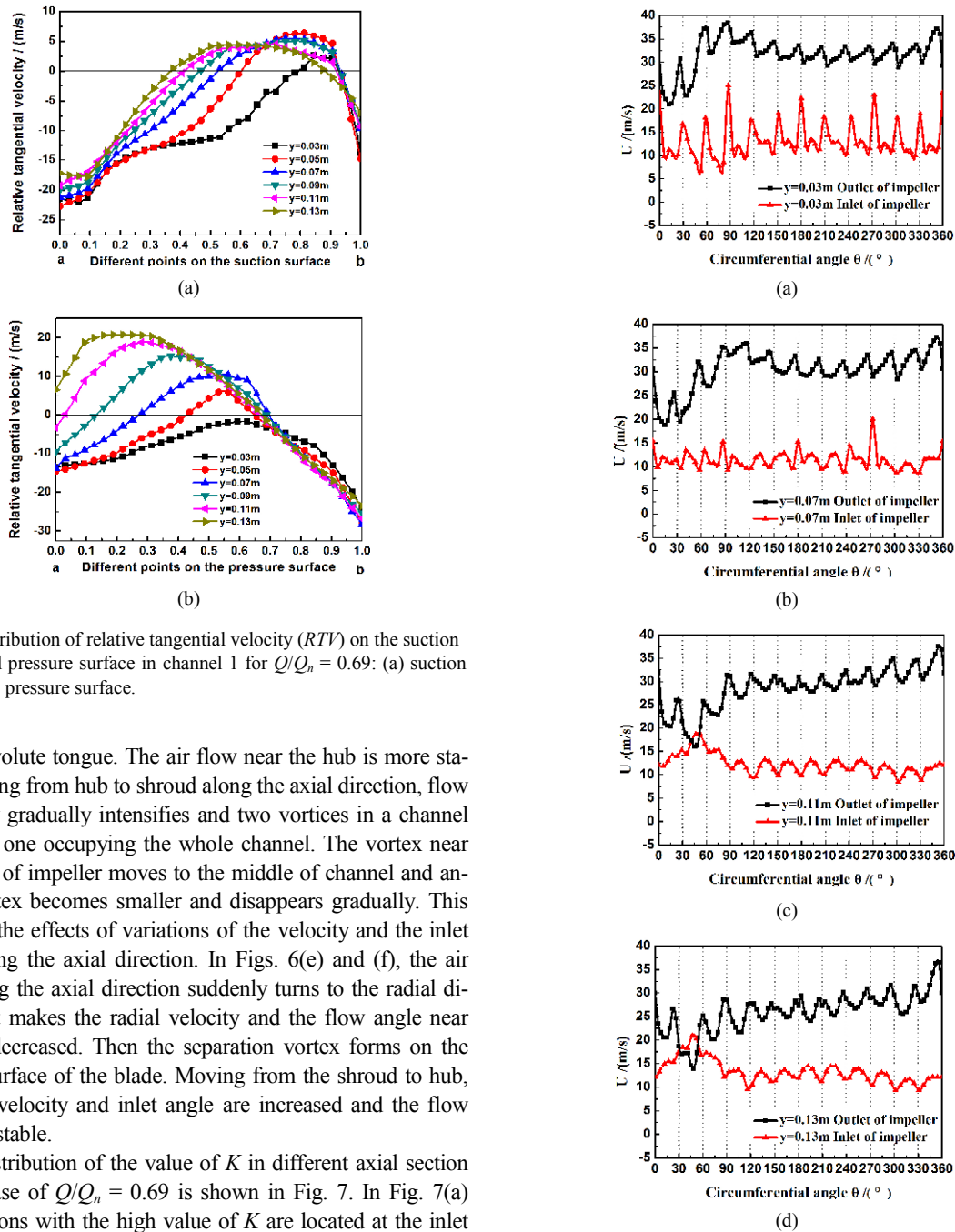
(a)

(b)

Fig. 8. Distribution of relative tangential velocity (*RTV*) on the suction surface and pressure surface in channel 1 for $Q/Q_n = 0.69$: (a) suction surface; (b) pressure surface.

near the volute tongue. The air flow near the hub is more stable. Moving from hub to shroud along the axial direction, flow instability gradually intensifies and two vortices in a channel reduce to one occupying the whole channel. The vortex near the outlet of impeller moves to the middle of channel and another vortex becomes smaller and disappears gradually. This is due to the effects of variations of the velocity and the inlet angle along the axial direction. In Figs. 6(e) and (f), the air flow along the axial direction suddenly turns to the radial direction. It makes the radial velocity and the flow angle near the hub decreased. Then the separation vortex forms on the suction surface of the blade. Moving from the shroud to hub, the flow velocity and inlet angle are increased and the flow becomes stable.

The distribution of the value of *K* in different axial section for the case of $Q/Q_n = 0.69$ is shown in Fig. 7. In Fig. 7(a) three regions with the high value of *K* are located at the inlet of unstable channels, the trailing edge of suction plate of unstable channels and the volute tongue, respectively. In the section of $y = 0.05$ m in Fig. 7(b), the areas with the high value of *K* at the outlet of impeller spread to surrounding regions and occupy the whole exit. Moving from the hub to the shroud, the value of *K* near the outlet of channel 3 is large, as shown in Figs. 7(c)-(e), which is in agreement with the change of streamlines in channel 3. The area with the high value of *K* also appears at the outlet of impeller in channel 4 in Fig. 7(f). To sum up, the location where *K* is large is consistent with the unstable zone in the flow field.

Fig. 8 shows the distribution of Relative tangential velocity (*RTV*) on the suction surface and pressure surface in channel 1.

(a)

(b)

(c)

(d)

Fig. 9. Distribution of velocity at the inlet and outlet of impeller in different sections for $Q/Q_n = 0.69$: (a) $y = 0.03$ m; (b) $y = 0.07$ m; (c) $y = 0.11$ m; (d) $y = 0.13$ m.

According to the definition of the relative tangential velocity, if the value of relative tangential velocity changes from negative to positive, the flow direction changes, indicating boundary layer separation occurs. From Fig. 8(a), all the maxima of relative tangential velocity in six sections are positive, namely, boundary layer separation occurs on the suction surface in six sections. The distance between two intersection points of the *RTV* curve and the curve of *RTV* = 0 is in agreement with the length of separation vortex. So it is found from the distance
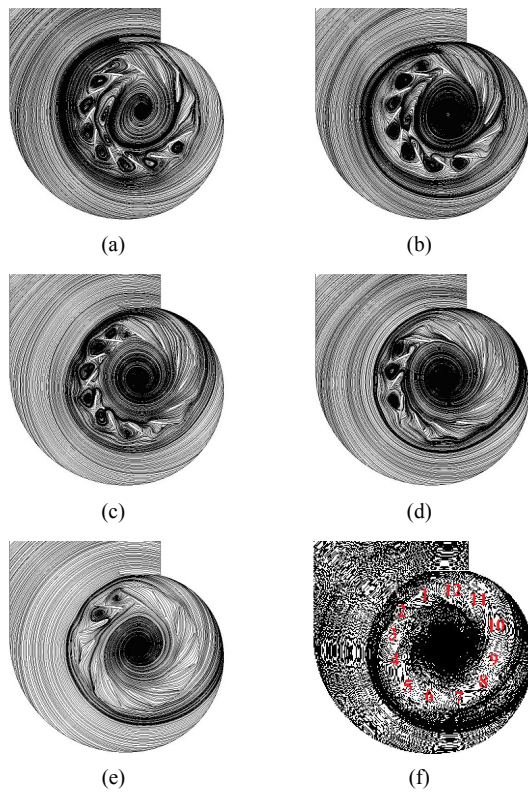
Fig. 10. Streamlines in the section of $y = 0.13$ m with increasing flow rate: (a) $Q/Q_n = 0.036$; (b) $Q/Q_n = 0.17$; (c) $Q/Q_n = 0.34$; (d) $Q/Q_n = 0.51$; (e) $Q/Q_n = 0.69$; (f) $Q/Q_n = 1$.

Fig. 11. K in the section of $y = 0.13$ m with increasing flow rate: (a) $Q/Q_n = 0.036$; (b) $Q/Q_n = 0.17$; (c) $Q/Q_n = 0.34$; (d) $Q/Q_n = 0.51$; (e) $Q/Q_n = 0.69$; (f) $Q/Q_n = 1$.

between two intersection points that the area of backflow region is small on the suction surface in section $y = 0.03$ m and it is larger in section $y = 0.13$ m. On the pressure surface, boundary layer separation occurs in most sections except $y = 0.03$ m. Comparing Figs. 8(a) and (b), the location of the boundary layer separation on the suction surface is near the outlet of flow channel and it is near the inlet of impeller on the pressure surface.

Fig. 9 is the distribution of velocity magnitude at the inlet and outlet of impeller in different sections for $Q/Q_n = 0.69$. From the physical meaning of two curves, the area between two curves is proportional to the flow rate through the impeller. Moving from hub to shroud, the area between two curves becomes small and the flow rate decreases. As shown in Figs. 9(c) and (d), the velocity at the outlet of impeller is lower than that at the inlet of impeller in channel 2 (30°-60°). It means the energy of air gained from the rotating impeller is less than the energy loss caused by the unstable phenomenon and fluid viscosity in channel 2. For the distribution of velocity at the impeller inlet, the fluctuation amplitude of velocity is reduced from hub to shroud. The velocity magnitude at the inlet of impeller in channels 1, 2 and 3 increases obviously, especially in channel 2. This is because the vortices in the above channels occupy the whole channels and the high speed air at the outlet of impeller is mixed with the low speed air at the impel-
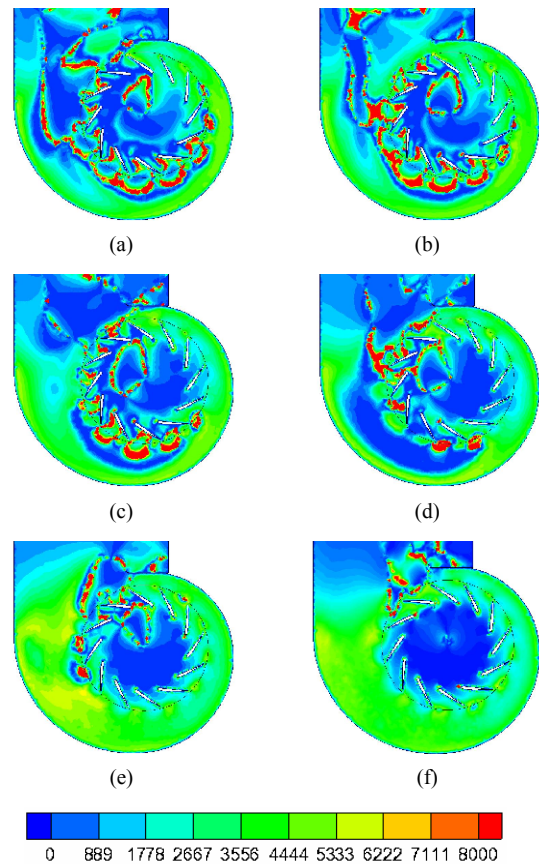
ler inlet, then the flow at the inlet of impeller accelerates and the flow at the outlet of impeller decelerates. The vortex in channels 1, 2 and 3 blocks the air flow and the fluid is pushed to the nearby channels. So the velocity at the impeller inlet in channel 2 increases greatly.

Fig. 10 shows the streamlines in the axial section of $y = 0.13$ m with increasing flow rate. One can see from the above discussion on the flow behavior of different axial sections that the fluid flow near the shroud more easily loses its stability, so the axial section of $y = 0.13$ m is chosen in the following analysis. The streamlines in the flow field are smooth and there is no instability zone for the case of $Q/Q_n \geqslant 1$. In Fig. 10(f), the streamlines at the outlet of channel 1 first tend to be unsmooth. With the decrease of flow rate, a vortex appears in channels 1 and 2 and the streamlines in channel 3 become bending in Fig. 10(e). As shown in Fig. 10(d), the strength of the vortex is weakened and the vortex disappears gradually in channel 1. The flow in channels 3 and 4 loses its stability and forms an obvious vortex. The streamlines in channels 5 and 6 begin to bend, which is the same with the flow change of channel 3 in Fig. 10(e). With the further reducing of flow rate, the strength of the vortex is enhanced and the size becomes larger. The flow at the outlet of channel 7 begins to be unsta-
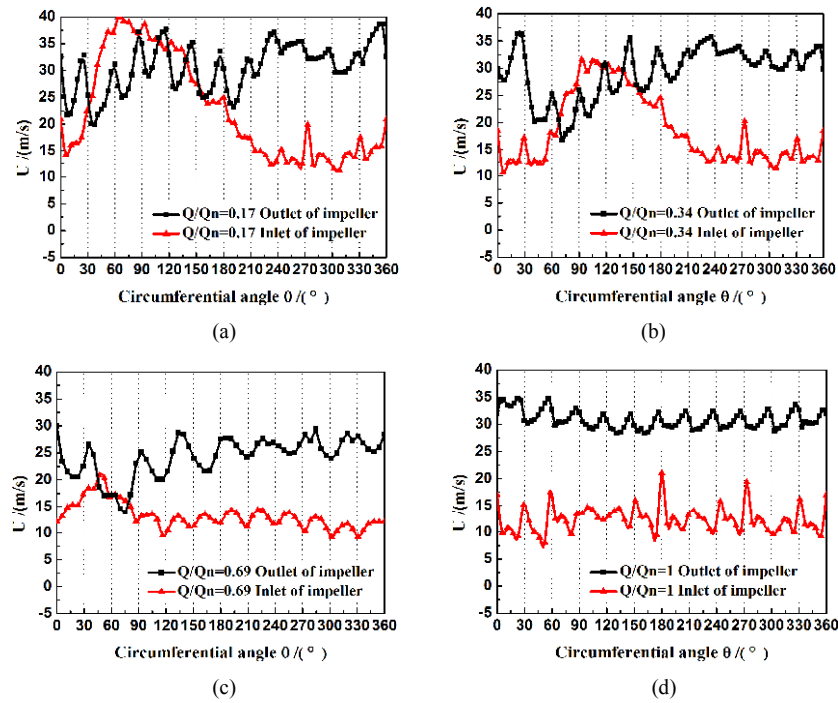
Fig. 12. Distribution of velocity at the inlet and outlet of impeller with different flow rate conditions in the section of $y = 0.13$ m: (a) $Q/Q_n = 0.17$; (b) $Q/Q_n = 0.34$; (c) $Q/Q_n = 0.69$; (d) $Q/Q_n = 1$.

ble for $Q/Q_n = 0.34$. As shown in Figs. 10(a) and (b), flow instability appears in the majority of channels and the number of the unstable channels is still on the rise.

In summary, flow in the channel near the volute tongue first loses its stability for the case of $Q/Q_n \leqslant 1$, namely, the volute tongue has a certain influence on the occurrence of flow instability. The separation vortex spreads along the opposite direction with rotating impeller. In the same channel, instability first occurs at the outlet of impeller and spreads to the inlet with the decrease of flow rate. When the flow rate is less than design value, the flow angle is not equal to the installation angle of blade, which would lead to the boundary layer separation on the suction plate of the blade. The formation of a vortex would make the flow channel blocked. In this case, the flow is forced to spread into the adjacent channels and the flow angle of the adjacent channels is changed, which is easy to cause boundary layer separation.

The distribution of the value of K in the section of $y = 0.13$ m with increasing flow rate is shown in Fig. 11. From the comparison of Figs. 10 and 11, the areas of high K value in Fig. 11 correspond to the regions where the separation vortex occurs in Fig. 10. The "jet-wake" structure is formed at the outlet of impeller due to the secondary flow between the suction surface and pressure surface. The shear layer between the jet flow and wake flow is very unstable. And at the same time, the value of K is very large at the outlet of the unstable channels.

Fig. 12 shows the distribution of velocity magnitude at the inlet and outlet of impeller with increasing flow rate. We can

see from Fig. 12(d) that the distribution of velocity at the inlet and outlet of impeller is relatively smooth and the air flow through every channel is almost the same when the flow rate is larger than the design value. At the condition of $Q/Q_n = 0.69$, the velocity at the outlet of impeller in channels 1, 2 and 3 becomes very low, while the velocity at the inlet of impeller changes little. With the further decrease of flow rate, the inlet velocity in the unstable channels accelerates and the outlet velocity decelerates, as shown in Figs. 12(a) and (b). In some channels, the velocity at the outlet of impeller is even lower than that at the inlet of impeller. That is due to the blend of different velocity air in the unstable channels.

Fig. 13 is the distribution of relative tangential velocity in the section of $y = 0.13$ m in channel 1. From Fig. 13(b), the maximum of relative tangential velocity on the suction surface happens to be zero, which implies the occurrence of boundary layer separation. At the same time, the value of relative tangential velocity on the pressure surface is lower than zero, which shows no reflow occurs. So the flow on the suction surface is easier to be unstable than that on the pressure surface. Similarly, the maxima of relative tangential velocity on both suction surface and pressure suction are positive in Fig. 13(a). So the separation vortex appears in channel 1, which is consistent with the flow behavior in Fig. 10(e) and the distribution of the high value of K in Fig. 11(e). Comparing two curves in Fig. 13(a), the region of backflow on the pressure surface is larger than the suction surface. As shown in Figs. 13(c) and (d), all the values of the relative tangential velocity on both suction surface and pressure suction are negative. This
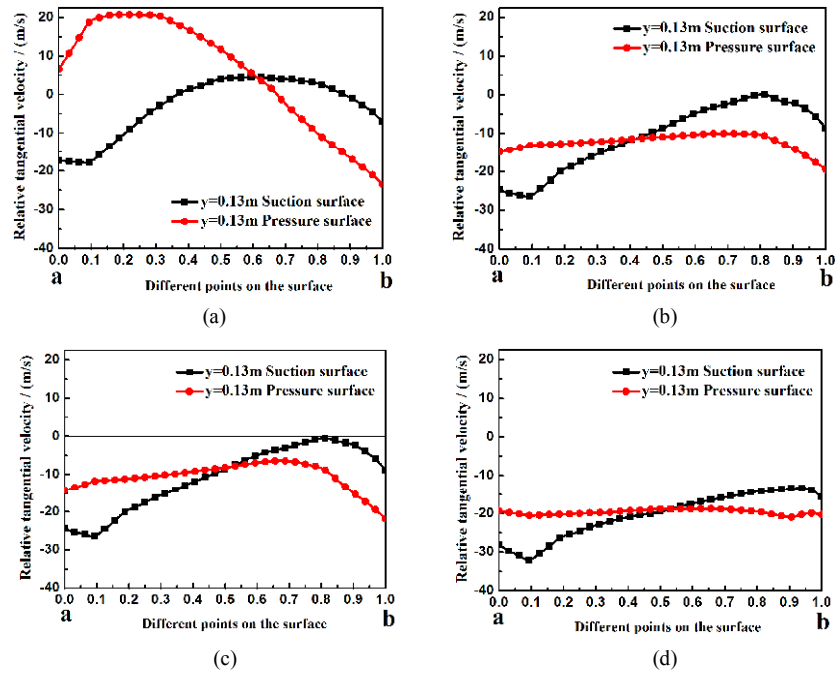
Fig. 13. Curves of relative tangential velocity in the section of $y = 0.13$ m in channel 1: (a) $Q/Q_n = 0.69$; (b) $Q/Q_n = 0.89$; (c) $Q/Q_n = 1$; (d) $Q/Q_n = 1.15$.
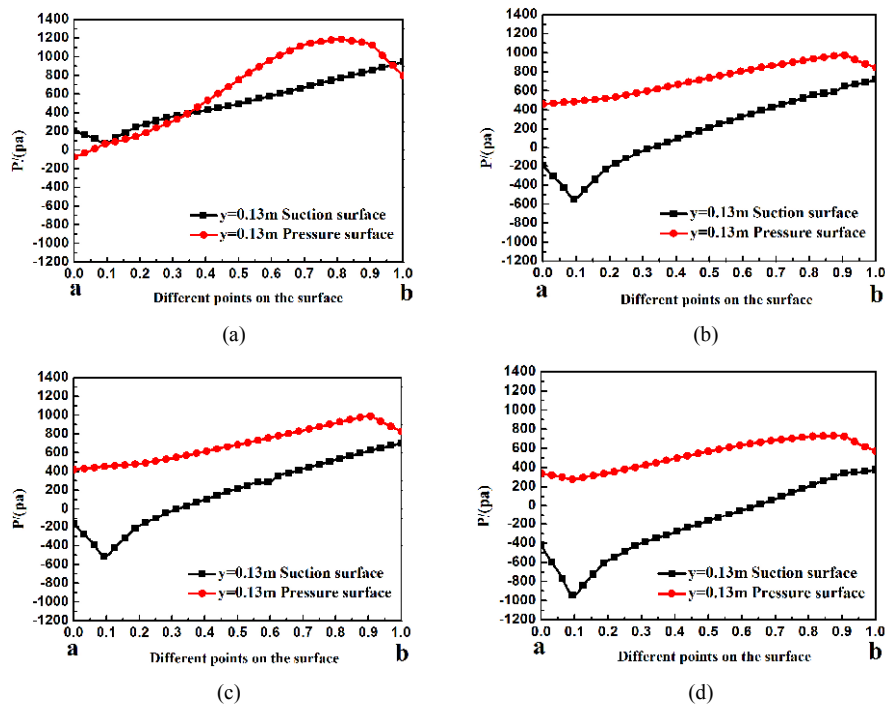

Fig. 14. Static pressure in the section of $y = 0.13$ m in channel 1: (a) $Q/Q_n = 0.69$; (b) $Q/Q_n = 0.89$; (c) $Q/Q_n = 1$; (d) $Q/Q_n = 1.15$.

indicates the flow in channel 1 is stable without boundary layer separation.

With the decrease of flow rate, boundary layer separation first occurs near the trailing edge of the suction surface and then it occurs at the entrance section of pressure surface. The absolute value of the relative tangential velocity both on the pressure surface and suction surface first gradually decreases, and then increases with the decrease of flow rate.

Fig. 14 shows the distribution of static pressure in the section of $y = 0.13$ m in channel 1. In Figs. 14(b)-(d), when boundary layer separation does not occur, the static pressure on the pressure surface is significantly greater than that on the

suction surface. The minimum of pressure on the suction surface is near the impeller inlet, and the maximum pressure on the pressure surface is near the outlet of the impeller. The pressure on the suction surface and pressure surface increases from the impeller inlet to the outlet. As shown in Fig. 14(a), when boundary layer separation occurs, two pressure curves cross near the inlet of impeller. From the comparison of four charts in Fig. 14, the pressure on the suction surface increases greatly and the pressure on the pressure surface near the inlet of impeller drops with the decrease of flow rate.

6. Conclusions

The air flow in the centrifugal fan was simulated in this study. The Navier-Stokes equations and RNG k-ε turbulent model describe the flow field and flow parameters are calculated by the finite volume method and SIMPLE algorithm. The flow behavior in the centrifugal fan and the distribution of the energy gradient function K are obtained at different flow rates and different axial sections. The main conclusions are as follows.

(1) The air flow near the hub is more stable than that near the shroud, due to the effects of variations of velocity and inlet flow angle.

(2) With the decrease of flow rate, the boundary layer separation first occurs near the trailing edge of suction surface and then at the entrance section of pressure surface.

(3) With the decrease of the flow rate, the instability zones in the same channel move to the impeller inlet from the outlet, and the separation vortex in different channels spreads in opposite direction to the rotation of impeller.

(4) According to the energy gradient method, the area with larger value of K is in agreement with unstable zones.

(5) The instability first occurs on the suction surface of flow channel near the volute tongue.

It is indicated that the energy gradient theory can be applied to analyze the flow instability in the centrifugal fan. In addition, the present result is useful to reveal the mechanism of the complex flow phenomena in centrifugal fans.

Acknowledgment

References

[1] G. R. Denger and M. Bride, Fluid measurement and instrumentation forum, *ASME* (1990) 49-56.

[2] V. S. Sandra, B. T. Rafael and S. M. Carlos, Unsteady flow pattern characteristics downstream of a forward-curved blade centrifugal fan, *ASME, J. of Fluids Engineering*, 123

(6) (2001) 265-270.

[3] Z. C. Zhu et al., Improvement on the method of aerodynamic design of impeller of centrifugal fan, *Compressor Blower & Fan Technology*, 3 (2001) 3-8.

[4] K. Q. Wu and J. Huang, Numerical analysis of vortex flow in the volute of centrifugal fan, *J. of Engineering Thermophysics*, 22 (3) (2001) 316-319.

[5] X. H. Chen et al., The improvement of the design of centrifugal fan using three- dimensional numerical simulation, *Compressor Blower & Fan Technology*, 2 (2003) 6-8.

[6] H. Tamaki, Effect of piping systems on surge in centrifugal compressors, *JMST*, 22 (2008) 1857-1863.

[7] K. J. Kang, J. G. Park and Y. H. Shin, Flow characteristics with variations of cut-off angle of multi-blade fan for ventilation, *The 10th Asian International Conference on Fluid Machinery* (2010) 732-739.

[8] K. Morinushi, The influence of geometric parameters of forward-curved centrifugal fan noise, *J. of Vibration, Acoustics, Stress, and Reliability in Design*, 109 (3) (1987) 227-234.

[9] P. N. Son, J. Kim and E. Y. Ahn, Effects of bell mouth geometries on the flow rate of centrifugal blowers, *JMST*, 25 (9) (2011) 2267-2276.

[10] P. N. Son, J. W. Kim, S. M. Byun and E. Y. Ahn, Effects of inlet radius and bell mouth radius on flow rate and sound quality of centrifugal blower, *JMST*, 26 (5) (2012) 1531-1538.

[11] J.-H. Kim, K.-H. Cha and K.-Y. Kim, Parametric study on a forward-curved blades centrifugal fan with an impeller separated by an annular plate, *JMST*, 27 (6) (2013) 1589-1595.

[12] H. Tamaki, Study on flow fields in high specific speed centrifugal compressor with unpinched vaneless diffuser, *JMST*, 27 (6) (2013) 1627-1633.

[13] L. Ding et al., Experimental and numerical analysis on the effect of inlet distortion on the performance of a centrifugal fan with a mixing chamber, *JMST*, 27 (2) (2013) 421-428.

[14] A. Jaatinen-Värri, P. Röyttä, T. Turunen-Saaresti and A. Grönman, Experimental study of centrifugal compressor vaneless diffuser width, *JMST*, 27 (4) (2013) 1011-1020.

[15] Y.-J. Kee and S.-J. Shin, Structural dynamic modeling for rotating blades using three dimensional finite elements, *JMST*, 29 (4) (2015) 1607-1618.

[16] H.-S. Dou, Mechanism of flow instability and transition to turbulence, *International J. of Non-Linear Mechanics*, 5 (41) (2006) 512-517.

[17] H.-S. Dou, Physics of flow instability and turbulent transition in shear flows, *International J. of Physical Science*, 6 (6) (2011) 1411-1425.

[18] H.-S. Dou, B. C. Khoo and K. S. Yeo, Instability of Taylor-Couette flow between concentric rotating cylinders, *International J. of Thermal Sciences*, 47 (2008) 1422-1435.

[19] H.-S. Dou and A. Q. Ben, Simulation and instability study of the flow around a cylinder between two parallel wall, *J. of Thermal Science*, 24 (2) (2015) 140-148.

Meina Xiao received her M.S. from Zhejiang Sci-Tech University in 2013. Since then, she has been a Ph.D. student in the Faculty of Mechanical Engineering and Automation at Zhejiang Sci-Tech University. Her research interests include computational fluid dynamics, fluid mechanics and turbomachinery.

Hua-Shu Dou received his Ph.D. from Beijing University of Aeronautics and Astronautics in 1991. Since 2011, he has been a professor in the Faculty of Mechanical Engineering and Automation at Zhejiang Sci-Tech University. His main areas of interest are computational fluid dynamics, fluid mechanics, aerodynamics, turbomachinery, non-Newtonian fluid mechanics as well as combustion and detonation.